

Article

Experimental and Numerical Study on Tensile Behavior of Double-Twisted Hexagonal Gabion Wire Mesh

Yu-Liang Lin ^{1,*}, Peng-Fei Fang ¹, Xin Wang ², Jie Wu ³ and Guo-Lin Yang ¹

¹ School of Civil Engineering, Central South University, Changsha 410075, China; csufpf@163.com (P.-F.F.); yangguolin6301@163.com (G.-L.Y.)

² Shenzhen Municipal Engineering Corporation, Shenzhen 518000, China; smec_wx@163.com

³ Shenzhen Branch Office, China Nerin Engineering Co., Ltd., Shenzhen 518042, China; jie-wu@outlook.com

* Correspondence: linyuliang11@163.com

Abstract: Double-twisted hexagonal gabion wire mesh is a type of reinforced soil material that is used in gabion retaining walls to stabilize the soil slope in geotechnical engineering. In this study, a series of tensile tests were conducted to investigate the tensile behavior of hexagonal gabion wire mesh. Meanwhile, numerical models of gabion wire mesh were built to investigate the whole tensile loading-strain process. The influence of wire diameter, mesh width, and mesh length on the tensile strength of hexagonal gabion wire mesh were evaluated based on laboratory tests and numerical simulation. The quantitative relationship of tensile strength versus wire diameter, mesh width, and mesh length was typically fitted by a quadratic function, linear function, and monotonically decreasing exponential function. The numerical result presents a good consistency with those obtained from the experiment. The result of the loading-strain curve obtained by both experiment and simulation exhibits an “S” shape with a distinct serrated characteristic. The loading-strain curve can be divided into the following four stages: mesh distortion stage, wire stretching stage, overall yield stage, and wire fracture stage, which well reflects the tensile behavior of double-twisted hexagonal wire mesh. The tensile behavior of gabion wire mesh is influenced by the structure pattern of wire mesh and the mechanical characteristic of steel wire.



Citation: Lin, Y.-L.; Fang, P.-F.; Wang, X.; Wu, J.; Yang, G.-L. Experimental and Numerical Study on Tensile Behavior of Double-Twisted Hexagonal Gabion Wire Mesh. *Buildings* **2023**, *13*, 1657. <https://doi.org/10.3390/buildings13071657>

Academic Editors: Bingxiang Yuan, Yong Liu, Xudong Zhang and Yonghong Wang

Received: 27 April 2023

Revised: 14 June 2023

Accepted: 26 June 2023

Published: 28 June 2023



Copyright: © 2023 by the authors. Licensee MDPI, Basel, Switzerland. This article is an open access article distributed under the terms and conditions of the Creative Commons Attribution (CC BY) license (<https://creativecommons.org/licenses/by/4.0/>).

Keywords: double-twisted hexagonal wire mesh; tensile test; simulation model; loading-strain curve; mathematical equation

1. Introduction

A retaining structure is a widely used measure to stabilize the slope in geotechnical engineering [1–4]. A gabion retaining wall is a typical retaining structure for its excellent engineering characteristics and price advantage [5–9], and it consists of a series of layered gabion elements. The double-twisted hexagonal wire mesh is a basic material of gabion element. Consequently, it is a fundamental necessity to study the tensile behavior of double-twisted hexagonal wire mesh material to ensure the safety of the gabion structure. As for the gabion retaining wall, the soil behind the wall exerts an earth pressure on the back of the retaining wall, and the wire mesh pulls the wall face to ensure its stability, which indicates that the tensile strength is a key index of gabion wire mesh material in engineering design.

The laboratory tensile test is an essential way to obtain the mechanical characteristics of double-twisted gabion wire mesh. Muhunthan et al. [10] performed a series of strength tests on various fabrics and seaming configurations of hexagonal mesh material to discuss its engineering and technical details. Hsieh et al. [11] conduct a full-scale engineering test to discuss the mechanical behavior of wire mesh material with or without one-center cut wire mesh panels by tensile test and punch test. The tensile loading strain of hexagonal wire mesh is also studied by many scholars [12–14], and the test results indicate strongly nonlinear characteristics of a stress–stress relationship. Apart from that, the pull-out

characteristic of wire mesh material is also of concern for scholars by means of a pull-out test [15,16], and the compression characteristics of a gabion cage filled with gravel are obtained by compression test [17]. Due to the special structural shape of the gabion mesh, it is necessary to design a clamp to fix the gabion for regular quality control. Atanasovska et al. [18] developed a tool that allowed repeated testing of hexagonal steel wire mesh with different dimensions.

A numerical simulation is another method to study the tensile behavior of double-twisted gabion wire mesh effectively and powerfully [19–24]. Ferro [25] developed a numerical model of a hexagonal net by using finite bar elements, and the hexagonal net was assumed to be elastic. Gu et al. [26] modeled the gabion element by using linearly elastic-plastic characteristics and Mohr–Coulomb failure criteria. More recently, Grodecki [27] employed a finite element model to simulate a static tensile test on hexagonal wire mesh. Cazzani et al. [28] introduced a two-noded truss element to model the wire mesh. Mummadisinh et al. [29] used a beam element in 2-D plane strain analysis on the gabion basket. Priour [30] modeled the nets of the hexagonal mesh using triangular elements, and the reliability of the model was verified by comparing them with test results.

In this study, a tensile test was conducted on hexagonal grid specimens to investigate the stress–strain behavior of the material. The specimens of four types with different wire diameters and grid sizes were prepared, and a special clamp was designed to fix the gabion mesh. Thereafter, a stress–strain characteristic derived from the experiment was compiled into finite element software, and a two-dimensional finite element model was established to analyze the mechanical response of double-twisted hexagonal wire mesh. In addition, the influence of wire diameter, mesh size (length and width) on tensile strength, and deformation of material was analyzed based on finite element analysis. Finally, the tensile stress–strain curve of gabion wire mesh was fitted via mathematical formula.

2. Tensile Tests

A series of tensile loading tests were carried out to investigate the loading–displacement response of the double-twisted hexagonal gabion wire mesh with different mesh sizes and wire diameters. The tests were conducted based on ASTM A975 (2011). In a tensile test, a special clamp was designed to fix and pull the mesh specimen, as shown in Figure 1.

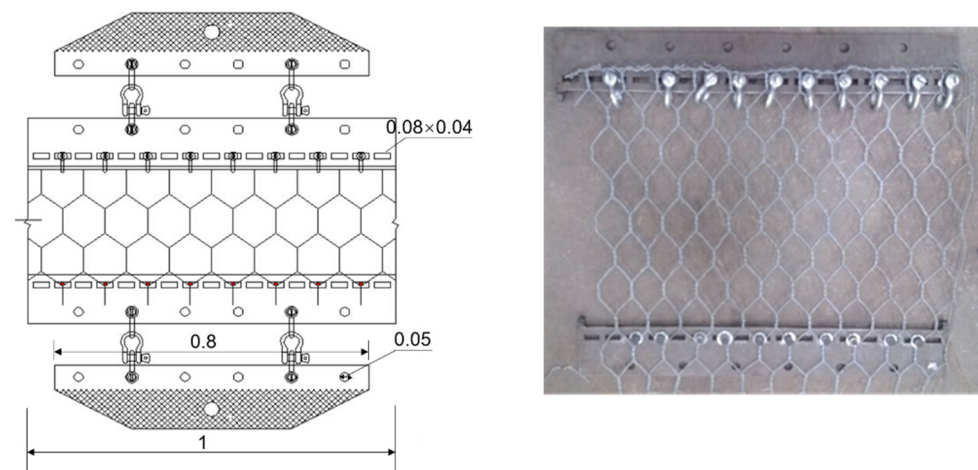


Figure 1. Clamp for gabion wire mesh.

2.1. Material

Double-twisted hexagonal wire mesh (as shown in Figure 2) is a woven structure made of galvanized steel wire, and the adjacent steel wire was interconnected to form a hexagonal opening. The hexagonal mesh, similar to the honeycomb structure, increased the macroscopic strength of the metal mesh, while the double strand could ensure that the entire hexagonal mesh surface keep its bearing capacity even if the single wire tensile

failed, and it could continue to withstand the loading. Selvedge wire was used to edge the mesh. Generally, the diameter of the selvedge wire was thick, which made the wire mesh more rigid.

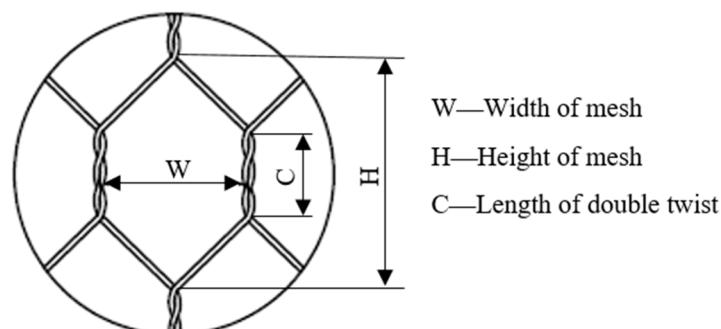


Figure 2. Basic shape of hexagonal wire mesh.

2.2. Scheme

Four types of hexagonal wire mesh with different mesh sizes and steel wire diameters were designed (as shown in Table 1) to evaluate the tensile behavior of gabion wire mesh. Three parallel measurements were conducted for each type of specimen to ensure the precision and reliability for determining a mean value. SHT4106G electro-hydraulic servo machine (as shown in Figure 3) was used in a tensile test. A constant strain rate of 1.25% strain/minute (5 mm/min) was adopted. The elongation and the applied loading are recorded automatically by the machine. A special clamp was designed to fix the gabion wire mesh and limit lateral deformation in the tensile test (see Figure 1). The clamp was composed of two steel plates that were connected by a shackle. Both ends of the clamp features a 45° and 135° scratch grid, which could provide sufficient friction. With the help of a special clamp, it was possible to investigate the overall wire mesh response considering the homogenized characteristics of mesh geometry.

Table 1. Basic size of four types of material specimen.

| Type | Mesh Opening Size | | Steel Diameter d (mm) | Selvedge Diameter (mm) | Number of Rib per Unit Length |
|------|-------------------|--------|--------------------------|---------------------------|----------------------------------|
| | W (mm) | H (mm) | | | |
| A | 60 | 80 | 2 | 2 | 14 |
| B | 60 | 80 | 2.2 | 2.7 | 14 |
| C | 82.5 | 122.5 | 2.2 | 2.7 | 14 |
| D | 82.5 | 122.5 | 2.7 | 3.4 | 14 |



Figure 3. Tensile machine (SHT4106G electro-hydraulic servo machine, MTS Systems China, Shanghai, China).

To make a comparison between the gabion mesh and single gabion wire, a series of tensile tests of single gabion wire were conducted. A photograph of the tensile experiment of a single steel wire is shown in Figure 4.



Figure 4. Tensile experiment testing of steel wire.

2.3. Results and Discussion

Among the three parallel measurements for each type of gabion mesh, the measured values are almost similar, which indicates that the test results are repeatable. The tensile test results of types A–D are typically shown in Figure 5. The stress–strain test results of gabion wire mesh are obviously nonlinear. The tensile stress–strain curves can be divided into four stages. The stress–strain curve is linear at Stages 1 and 2, and the slope of the curve at Stage 1 is smaller than that at Stage 2. At Stage 1, the elongation of gabion mesh is primarily induced by the strain of a single wire and the deformation of the hexagonal cell. At Stage 2, elongation of gabion mesh is mainly caused at the twisted-wire section. At Stage 3, there is a significant increase in strain, which is followed by a drop in tensile force, accompanied by a minor fluctuation. The phenomenon indicates that the wire mesh begins to yield, and the tensile force during this stage reaches the ultimate strength of the wire mesh material. At Stage 4, the tensile stress descends significantly and then continues to grow, which exhibits a distinct serrated shape. However, there is no obvious yield platform in the stress–strain curve of Type B due to a fracture failure of steel wire. The first peak values of tensile force occur, corresponding to the strain values of 20%, 16%, 18%, and 16% for types A, B, C, and D, respectively. After the tensile force reaches a peak value, a drop in tensile force occurs due to the fracture failure of a steel wire. Several similar consecutive peak tensile forces are observed after the first peak tensile force. Because the rest steel wires can still withstand tensile force, the tensile force continues to grow, and the stress distribution changes. The tensile stress–strain curve exhibits an ‘S’ shape during Stages 1 to 3, and a distinct serrated shape at Stage 4 is observed due to the fracture of steel wire.

Results of the tensile mechanical index for types A–D are listed in Table 2. The values of the tensile strength are 49.23 kN/m, 55.82 kN/m, 37 kN/m, and 40.77 kN/m for gabion wire mesh of types A–D, respectively. The tensile stress–strain responses of four types of wire mesh material are different due to different hexagonal cell sizes and wire diameters. In other words, the tensile stress–strain characteristics are significantly influenced by the hexagonal cell size and wire diameter.

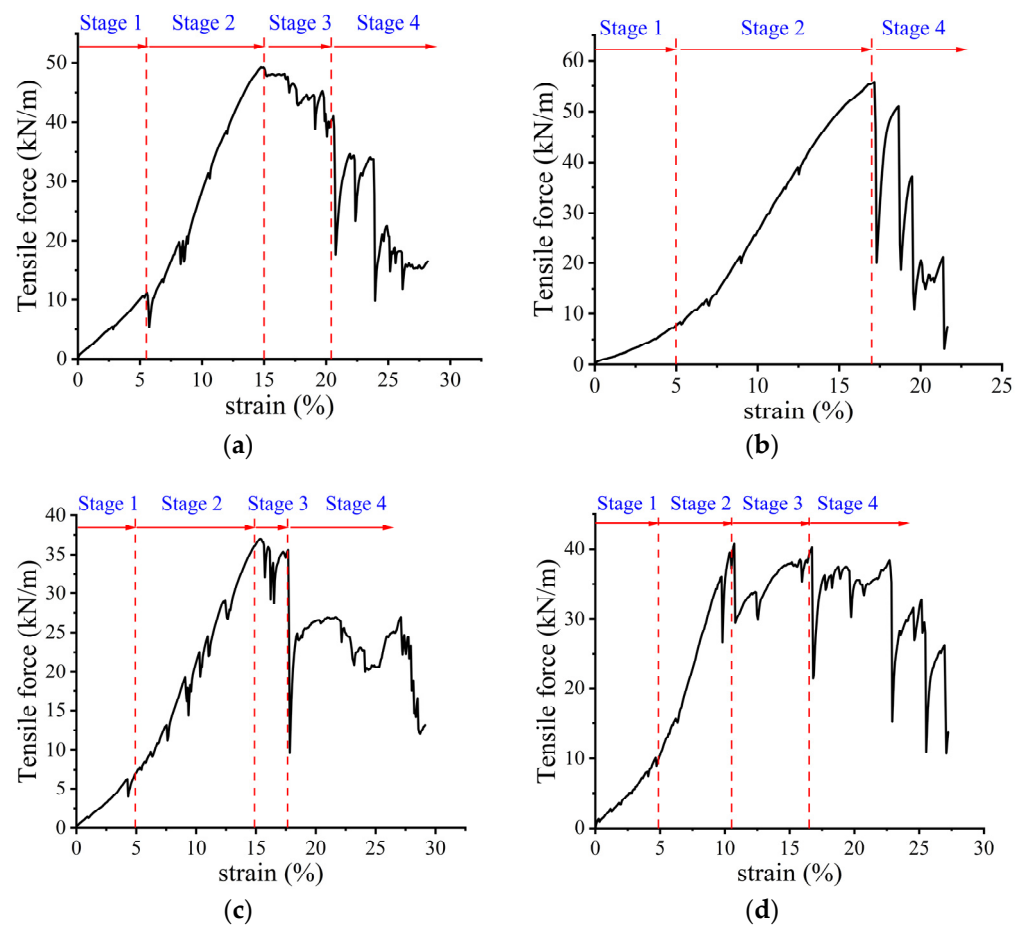


Figure 5. Stress–strain test results of gabion wire mesh material. (a) Type A; (b) Type B; (c) Type C; (d) Type D.

Table 2. Tensile strength at different strain values of gabion mesh material.

| Type | Tensile Strength 2% Strain (kN/m) | Tensile Strength 5% Strain (kN/m) | Tensile Strength 10% Strain (kN/m) | Tensile Strength Ultimate Strain (kN/m) |
|------|--------------------------------------|--------------------------------------|---------------------------------------|---|
| A | 4.16 | 10.05 | 28.29 | 49.23 |
| B | 2.62 | 7.85 | 26.36 | 55.82 |
| C | 2.58 | 7.16 | 21.23 | 37.00 |
| D | 3.61 | 10.54 | 35.10 | 40.77 |

2.3.1. Influence of Hexagonal Mesh Size

The diameters of gabion steel wire of types B and C are both 2.2 mm. The hexagonal mesh size of Type B is 60 mm × 80 mm, while it is 82.5 mm × 122.5 mm for Type C. Consequently, types B and C are selected to analyze the influence of mesh size on tensile strength.

By comparing the typical stress–strain curves of the tensile test of Type B and C (as shown in Figure 6), it is seen that the stress–strain curves show a similar gradient at Stage 1, which indicates a close elasticity modulus. At Stage 2, the tensile force of Type B grows faster than that of Type C, and the peak value of Type B is higher than that of Type C, which means that the tensile strength of Type C is smaller than that of Type B. The smaller mesh size will induce a larger tensile strength of gabion wire mesh. A larger mesh size would probably make the mesh structure pattern relatively sparse, and the strength value is not as large as that of mesh with small cells and a dense mesh structure. Meanwhile, the elongation between each consecutive break of Type B is significantly less than that of Type C at Stage 4, which implies that the wire mesh of Type B deforms less when subjected to

tensile loading. However, due to the limited number of material types in the tensile test, these two factors were not separately discussed here.

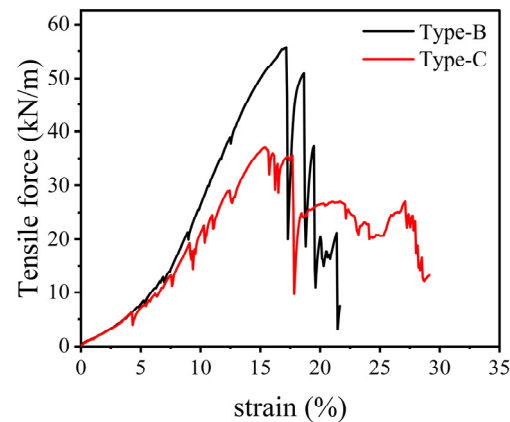


Figure 6. Tensile force–strain curve of gabion wire mesh with different mesh size.

2.3.2. Influence of Steel Wire Diameter

The same mesh size with different wire diameters is designed between types A and B, as well as between types C and D. Consequently, a typical comparison can be made between types A and B, types C and D, respectively, to analyze the influence of wire diameter on tensile behavior. The influence of wire diameter on stress–strain curve in the tensile test is typically shown in Figure 7. The curves at Stages 1 and 2 are quite similar. Types A and D have larger peak tensile stress than types B and C. A larger wire diameter causes a higher tensile strength of wire mesh, and a larger diameter also makes the wire mesh more rigid.

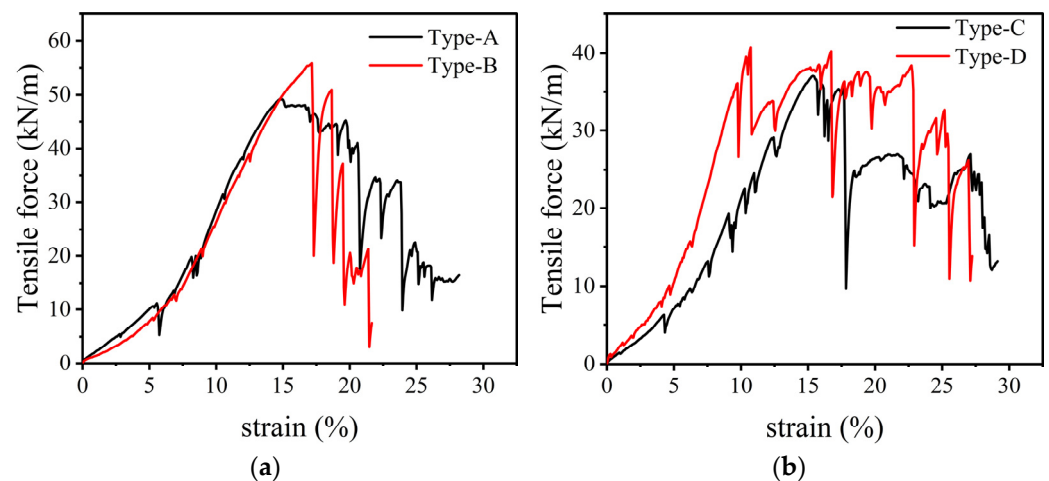


Figure 7. Tensile stress–strain response of gabion wire mesh with different wire diameter: (a) types A and B; (b) types C and D.

3. Numerical Modeling

A finite element model (FEM) is established to simulate the tensile test of hexagonal gabion wire mesh. Firstly, the numerical model is established based on the geometric model of the specimen with the aim to verify the effectiveness of the simulation. Thereafter, the numerical models with different structure patterns of mesh size and steel diameter are established to conduct a sensitivity analysis of geometric factors. Finally, mathematical models are put forward to simulate progressive damage and failure.

3.1. Numerical Model

3.1.1. Constitutive Behavior

The stress–strain curve of a single wire based on tensile test is shown in Figure 8. The single steel wire presents a nonlinear elasto-plastic characteristic. Consequently, an elastic-plastic model of stress–strain relationship was adopted to reflect the nonlinearity and plasticity of the material. A same stress–strain mode is used for double wire and selvedge wire with different cross-section areas. Moreover, the stress–strain relationship of double twist wire is not only determined by the tension strength of steel wire but also influenced by bending and shearing strength. Due to the difficulty of establishing a 3-D continuum element of the wire mesh, a 2-D beam model is simply applied to describe the behavior of wire. The beam element in ABAQUS is a “beam-column” element, which means that it allows axial, bending, and torsional deformation. The effect of transverse shear deformation is also considered in the Timoshenko beam element. A 2-node linear beam in a plane is adopted to simulate the wire mesh. The hybrid beam element is available in geometric nonlinearity and large deformation simulation. Each steel wire was divided into a series of elements, and it can produce acceptable results based on beam theory.

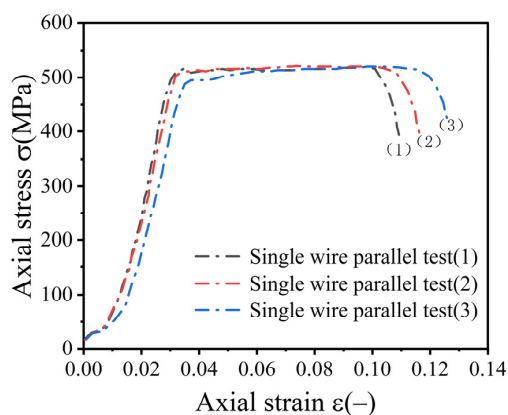


Figure 8. Stress-strain characteristic of single wire in tensile test.

Based on the platform of ABAQUS, the plastic data should be specified in terms of true stress and strain. Nevertheless, the tensile test only provides nominal (engineering) values of total stress and strain. Consequently, a procedure is needed to convert the nominal test data to true stress–strain relationship to decompose the total strain into elastic component and plastic component, respectively (see Figure 9). A conversion method is summarized by Hussein [31]. Based on tensile tests (see Figure 7), Young’s modulus (E), and the stress at failure (σ_f) were determined as $E = 130$ GPa, $\sigma_f = 520.36$ MPa. A Poisson’s ratio is 0.23 for the sheet material of gabion wire mesh [32]. The von Mises yield criterion is adopted, and the plastic properties of wire mesh are introduced into the ABAQUS platform.

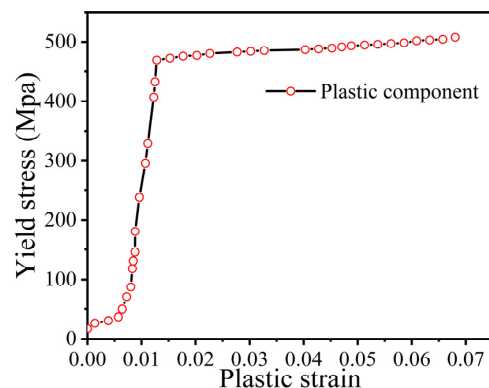


Figure 9. Decomposition of total strain.

3.1.2. Geometry and Boundary Conditions

A 2D model of a material sample of Type D is presented for validation, as shown in Figure 10. Model global size is $L_x = 660$ mm (perpendicular to the twist) and $L_y = 446$ mm (parallel to the twist). Hexagonal mesh size is $W = 82.5$ mm (Width) and $H = 122.5$ mm (Height). The cross-section of the wire was a circle with a diameter of 2.7 mm for single wire and 5.4 mm for twist wire. In the longitudinal direction (Y-Y), the wire mesh is restrained at the bottom side, and the displacement is applied from the opposite side with a constant strain rate of 1.25% strain/min.

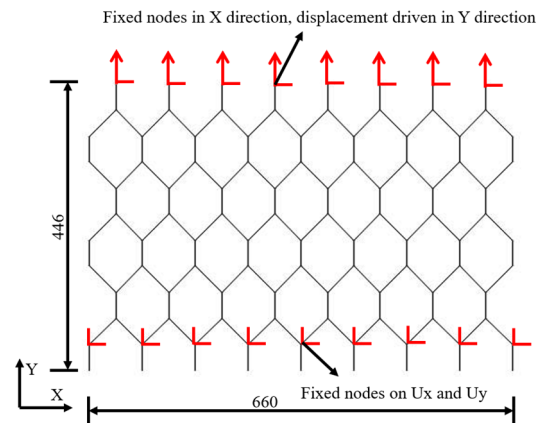


Figure 10. Geometry and boundary condition of FEM model.

3.2. Model Validation

The stress–strain behavior of wire mesh determined by numerical simulation was compared with that obtained in the tensile test, as shown in Figure 11. The changing trend of stress–strain curve in numerical simulation is found to be consistent with the experimental result, exhibiting a piece-wise linear and strengthening yield stage, although the numerical simulation cannot well reflect the stress–strain characteristics at the damage stage (i.e., Stage 4). As for the engineering design of gabion retaining wall, the gabion mesh material will not reach its yield strengthening stage due to a safety control. Consequently, the characteristic at Stage 4 can be ignored for the description of the tensile behavior of the gabion wire mesh material. Besides, the elastic modulus in numerical simulation is larger than that in the tensile test. The beam element is used to simulate the wire mesh, which may cause the entire model to become more rigid since the elastic–plastic model has a tendency to overestimate the stiffness of the mesh. In summary, the FEM model can effectively simulate the macroscopic nonlinear behavior of wire mesh before the wire mesh reaches its yield strength. However, the numerical simulation cannot reflect the zigzag features when the wire begins to fracture.

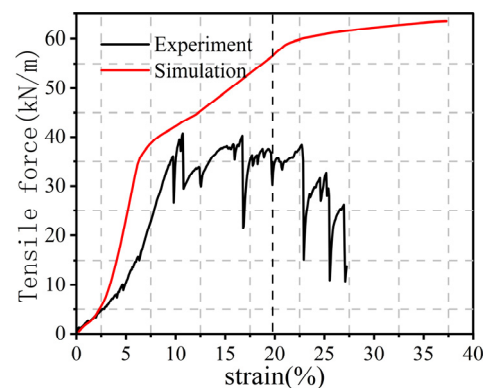


Figure 11. Comparison between experiment and simulation.

3.3. Tensile Characteristics

Figure 12 shows the deformation pattern of gabion wire mesh after applying a boundary displacement (U_y) of 80 mm at the model top. The deformation pattern of the wire mesh is consistent with the experimental results. Severe distortion of the hexagonal mesh shape at the edges is observed, while the shape of the grid in the middle changes slightly since the twisted wires bear most of the tensile force. With an increase in tensile force, the gabion wire mesh gradually narrows and eventually fails. Meanwhile, the displacement generally decreases as the distance to the applied loading increases, and it reaches zero at the fixed boundary.

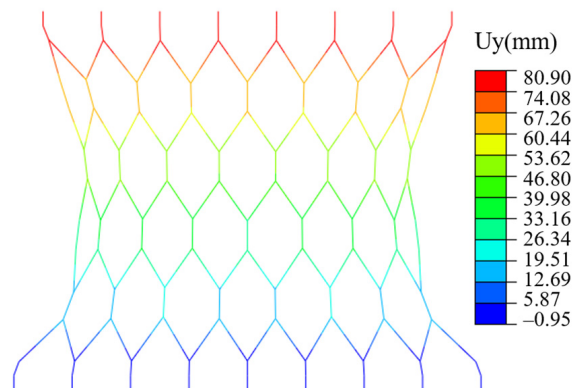


Figure 12. Displacement along wire mesh subjected to a boundary displacement ($U_y = 80$ mm).

The axial stress distribution subjected to an applied boundary displacement of 36 mm is shown in Figure 13. The axial stress is caused by both tensile and bending effects since a beam element is adopted in numerical simulation. In order to investigate the effect of tensile and bending effects separately, it is necessary to subtract the bending stress from axial stress, and then the tension stress can be obtained. A couple of gabion mesh are twisted together, and they are numbered from 1 to 7 (see Figure 13), and the axial stress (S_{11}) of each steel wire is listed in Table 3. It is seen that the steel wire in the middle of the gabion mesh is subjected to a greater tensile force. And therefore, the steel wire of hexagonal gabion mesh in the middle will first reach the yield condition, and the yield area gradually moves towards the outer side of the gabion mesh. At the yield stage, the wire mesh undergoes a continuous stress redistribution. The distribution of stress parallel to the loading direction is almost uniform when it reaches a certain displacement loading. Due to a stress concentration at the loading point of the boundary, the result is scattered on the boundary.

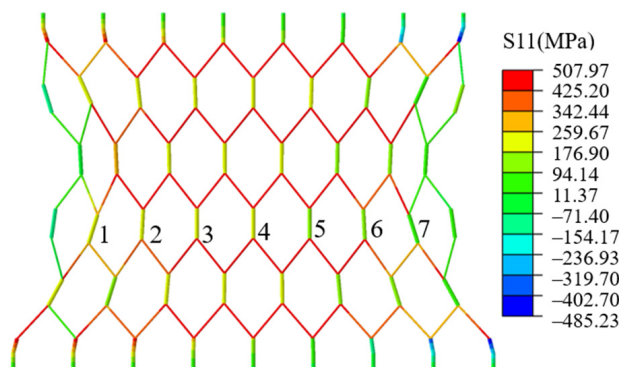
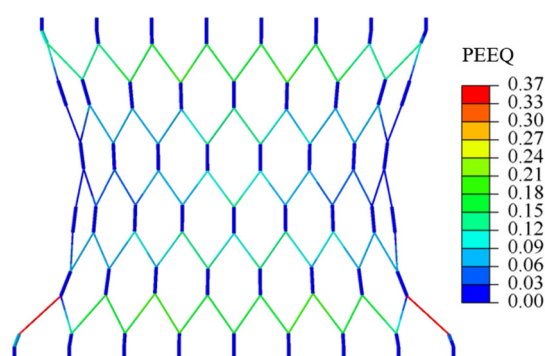


Figure 13. Axial stress of wire subjected to an applied boundary displacement ($U_y = 36$ mm).

Table 3. Stress of steel wire in gabion.

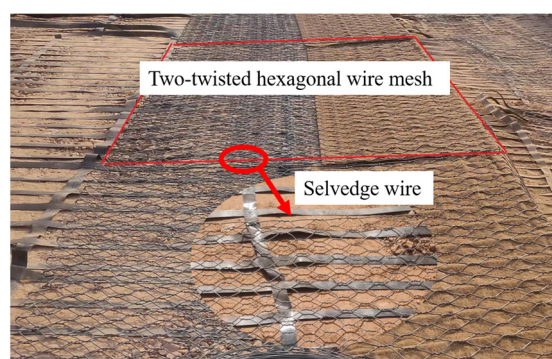
| Wire Number | Axial Stress (MPa) | Tensile Stress (MPa) |
|-------------|--------------------|----------------------|
| 1 | 197 | 130 |
| 2 | 212 | 167 |
| 3 | 189 | 168 |
| 4 | 176 | 176 |
| 5 | 147 | 168 |
| 6 | 122 | 167 |
| 7 | 63 | 130 |

The equivalent plastic strains (PEEQ) are adopted to reflect the yield area of gabion mesh subjected to tensile loading, as shown in Figure 14. It is evident that plastic strain is concentrated on the single steel wire.

**Figure 14.** Distribution of plastic strain (PEEQ).

3.4. Sensitivity Analysis

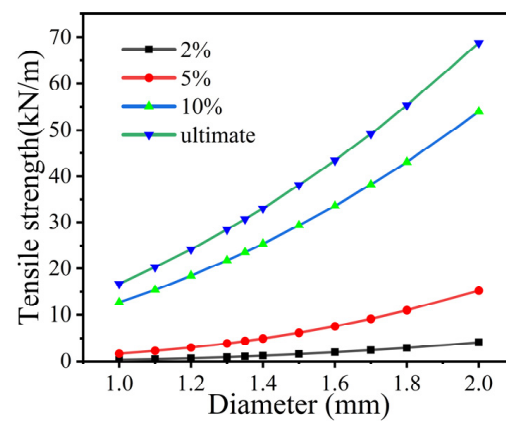
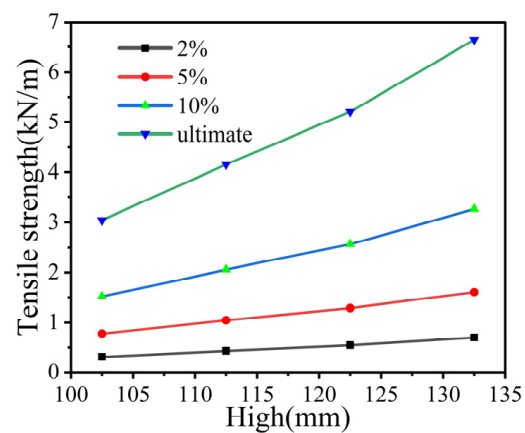
The influence of hexagonal mesh size and wire diameter on the tensile strength of gabion wire mesh can be qualitatively analyzed. Figure 15 shows a picture of gabion wire mesh in engineering practice. Accordingly, a finite element model is established, and the selvedge wires are considered in the numerical model.

**Figure 15.** Wire mesh in engineering practice.

Eighteen types of gabion mesh with different structure patterns are simulated in numerical analysis, as shown in Table 4. Tensile strength is measured at the following four different strains: 2%, 5%, 10%, and ultimate strain. Figures 16–18 show the influence of wire diameter, mesh height, and mesh width on the tensile strength of gabion mesh. The tensile strength increases nonlinearly as the wire diameter increase, and the relationship can be well-fitted by a quadratic function. The tensile strength almost linearly increases as the mesh height increases. However, the tensile strength is inversely proportional to the mesh width, with a monotonic decrease as the mesh width increases.

Table 4. Influence of structure patterns on tensile strength of gabion mesh.

| Types of Gabion Mesh | Factors | | |
|----------------------|--------------------|-----------------|------------------|
| | Wire Diameter (mm) | Mesh Width (mm) | Mesh Height (mm) |
| 1 | 1.00 | 82.5 | 122.5 |
| 2 | 1.10 | 82.5 | 122.5 |
| 3 | 1.20 | 82.5 | 122.5 |
| 4 | 1.35 | 82.5 | 122.5 |
| 5 | 1.40 | 82.5 | 122.5 |
| 6 | 1.50 | 82.5 | 122.5 |
| 7 | 1.60 | 82.5 | 122.5 |
| 8 | 1.70 | 82.5 | 122.5 |
| 9 | 1.80 | 82.5 | 122.5 |
| 10 | 2.00 | 82.5 | 122.5 |
| 11 | 1.35 | 82.5 | 102.5 |
| 12 | 1.35 | 82.5 | 112.5 |
| 13 | 1.35 | 82.5 | 122.5 |
| 14 | 1.35 | 82.5 | 132.5 |
| 15 | 1.35 | 62.5 | 122.5 |
| 16 | 1.35 | 72.5 | 122.5 |
| 17 | 1.35 | 82.5 | 122.5 |
| 18 | 1.35 | 92.5 | 122.5 |

**Figure 16.** Influence of wire diameter.**Figure 17.** Influence of mesh height.

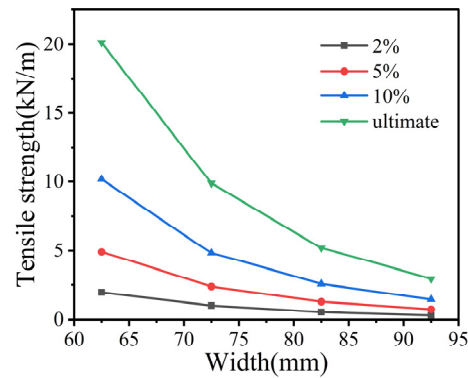


Figure 18. Influence of mesh width.

4. Mathematical Description

In order to establish a suitable mathematical model for the tensile stress–strain relationship, typical mathematical formulas are adopted to fit the tensile dataset of experiment and numerical simulation. Several typical mathematical models have been developed to model the woven material. Bergado et al. [33] proposed a model to describe the behavior of hexagonal mesh, and it was suitable for some specific cases. Vangheluwe [34] proposed a nonlinear three-element model to fit the tensile stress–strain characteristics of weave yarns based on a Maxwell element. The nonlinear three-element model is shown in Figure 19. The basic component of the nonlinear three-element model includes two nonlinear spring elements and one Maxwell element.

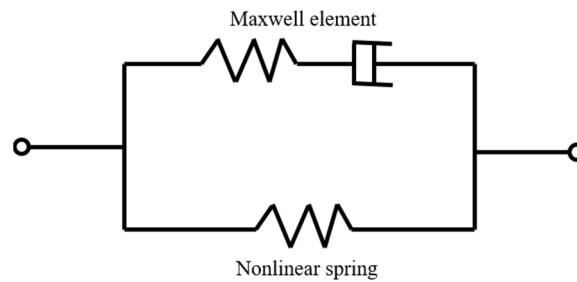


Figure 19. Nonlinear three element model.

The mathematical formula for nonlinear spring:

$$\sigma = b\varepsilon^2 \quad (1)$$

where, b is the spring constant of nonlinear spring.

The mathematical formula for Maxwell element:

$$\sigma = \eta\varepsilon \quad (2)$$

where, η is the viscosity of dashpot of Maxwell element.

The differential Equation (3) governs the tensile behavior of material.

$$\frac{d\sigma}{dt} + \frac{E}{\eta}\sigma = (E + 2b\varepsilon)\frac{d\varepsilon}{dt} + \frac{Eb}{\eta}\varepsilon^2 \quad (3)$$

where, σ and ε are stress and strain of the model respectively; E is a spring constant.

As the tensile test adopts a constant rate of extension, Equation (3) can be solved with $\varepsilon = kt$ and initial condition of $\sigma(t = 0) = 0$. Subsequently, the solution of differential Equation (3) can be solved as follows:

$$\sigma = k\eta\left(1 - e^{-\frac{E\varepsilon}{k\eta}}\right) + b\varepsilon^2 \quad (4)$$

The parameters in Equation (4) reflect the physics of nonlinear three-element model. However, Equation (4) cannot connect well to the tensile behavior of the gabion wire mesh since it can only reflect the first two stages of the stress–strain curve. The third stage of the tensile curve of the gabion mesh is also important. In this study, the yield stage is taken into account based on the real mechanical properties of the gabion wire mesh (Equation (5)).

$$\Sigma = A - Ae^{-\left(\frac{E\varepsilon}{k}\right)^\alpha} \quad (5)$$

where, E (Mpa) is the Elastic modulus of the wire steel. k (Mpa) is a constant related to the Elastic modulus. According to the fitting results, the range of k can be determined in a range of $1/0.14 \sim 1/0.2 E$. As for the gabion wire mesh, the value of k is $0.18 E$. α is a dimensionless correction coefficient, which can be selected within a range of 1.5–3, and it is 2.4 for the gabion wire mesh. Parameter A (kN/m) is the tensile strength of gabion mesh.

Assuming that the tensile strength of gabion mesh consists of the following two parts: one depends on the property of wire steel, and the other one depends on the hexagonal mesh size. The properties of wire steel are primarily determined by the wire diameter (d) and yield strength (σ_f), and the size of the hexagonal mesh is described by its width (W) and height (H). According to the sensitivity analysis of the influencing factors, the tensile strength of gabion mesh is proportional to the diameter of the wire, proportional to the width of the hexagonal mesh, and inversely proportional to the height of the hexagonal mesh. Consequently, Equation (6) was proposed to calculate the value of parameter A in polynomial form as follows:

$$A = \sigma_f \left(X_1 d + X_2 \frac{d^2}{W} + X_3 H \right) \quad (6)$$

where, X_1 , X_2 , and X_3 are scale factors. In order to determine scale factors, multiple linear regression is performed on 18 sets of datasets based on numerical simulation. The fitting results are listed in Table 5. The correlation coefficient R^2 is 0.999, which indicates an acceptable correlation.

Table 5. Multiple regression fitting results of scale factor.

| Symbol | Fitting Results | Standard Error | Correlation R^2 |
|--------|----------------------|--------------------|-------------------|
| X_1 | 0.091 | 0.012 | 0.999 |
| X_2 | 6.57 | 0.350 | |
| X_3 | 5.2×10^{-4} | 8×10^{-5} | |

A mathematical formula can be established to describe the tensile stress–strain of the double-twisted hexagonal gabion wire mesh as follows:

$$\sigma = \sigma_f \left(X_1 d + X_2 \frac{d^2}{W} + X_3 H \right) - \sigma_f \left(X_1 d + X_2 \frac{d^2}{W} + X_3 H \right) e^{-\left(\frac{E\varepsilon}{k}\right)^\alpha} \quad (7)$$

Thus, five material parameters, including wire elastic module, wire yield strength, wire diameter, hexagonal mesh width, and hexagonal mesh height, are considered in Equation (7).

A typical comparison between Equation (7) and the test result is shown in Figure 20. The zigzag features when the wire begins to fracture cannot be reflected by Equation (7). However, the theoretical stress–strain curve is consistent with the experimental result before the gabion mesh reaches its ultimate strength. In engineering design, the gabion mesh material will not reach its yield strengthening stage due to a safety factor, which is larger than 2.0. In this situation, the theoretical equation makes sense.

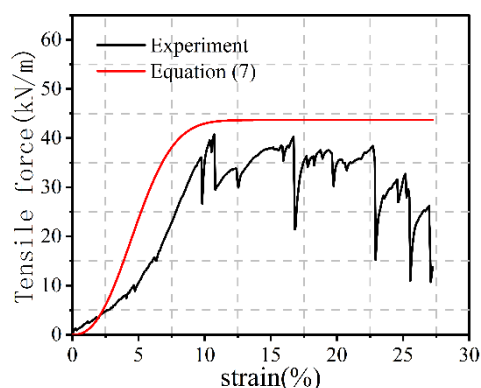


Figure 20. Comparison between the presented equation with the test results.

5. Conclusions

This paper conducts a series of tensile tests on double-twisted hexagonal gabion wire mesh to investigate its tensile behavior. Meanwhile, the numerical models are established based on stress–strain characteristic of gabion wire mesh. Moreover, a mathematical formula is established to describe the tensile behavior of gabion wire mesh. The main conclusions are summarized below.

The tensile stress–strain characteristic of gabion wire mesh is obviously nonlinear. The tensile stress–strain curve is divided into four stages, and it exhibits an “S” shape from Stage 1 to Stage 3. A distinct serrated shape is observed at Stage 4 due to the fracture of the steel wire. The failure of wire mesh initially exists near the center, and the failure area gradually moves towards the outer side. An increase in wire diameter or a decrease in mesh size causes the tensile strength to increase.

The numerical model is established to simulate the nonlinear characteristic of gabion wire mesh subjected to tensile loading based on experimentally measured tension data. The geometric properties of wire mesh play a main role in tensile behavior. The quantitative relationship of tensile strength versus three factors (wire diameter, mesh height, and mesh width) is established.

The mathematical formula is proposed to describe the tensile behavior of double-twisted hexagonal gabion wire mesh with consideration of shape and mechanical parameters. The mathematical formula can provide a reference for the design and engineering application of gabion structures.

Author Contributions: Conceptualization, Y.-L.L., P.-F.F., X.W., J.W. and G.-L.Y.; methodology, Y.-L.L., P.-F.F., X.W., J.W. and G.-L.Y.; validation, P.-F.F., X.W. and J.W.; formal analysis, P.-F.F.; investigation, P.-F.F., X.W. and J.W.; resources, Y.-L.L. and G.-L.Y.; data curation, Y.-L.L., P.-F.F. and G.-L.Y.; writing—original draft preparation, Y.-L.L. and P.-F.F.; writing—review and editing, Y.-L.L. and P.-F.F.; visualization, Y.-L.L. and P.-F.F.; supervision, Y.-L.L. All authors have read and agreed to the published version of the manuscript.

Funding: This research project was funded by the National Natural Science Foundation of Hunan Province, grant numbers 2021JJ30830.

Institutional Review Board Statement: Not applicable.

Informed Consent Statement: Not applicable.

Data Availability Statement: The data presented in this study may be available on reasonable request from the corresponding author.

Conflicts of Interest: The authors declare no conflict of interest.

References

1. Lin, Y.L.; Leng, W.M.; Yang, G.L.; Zhao, L.H.; Li, L.; Yang, J.S. Seismic active earth pressure of cohesive-frictional soil on retaining wall based on a slice analysis method. *Soil Dyn. Earthq. Eng.* **2015**, *70*, 133–147. [\[CrossRef\]](#)
2. Lin, Y.L.; Yang, G.L.; Yang, X.; Zhao, L.H.; Shen, Q.; Qiu, M.M. Response of gravity retaining wall with anchoring frame beam supporting a steep rock slope subjected to earthquake loading. *Soil Dyn. Earthq. Eng.* **2017**, *92*, 633–649. [\[CrossRef\]](#)
3. Lin, Y.L.; Zhao, L.H.; Yang, T.Y.; Yang, G.L.; Chen, X.B. Investigation on seismic behavior of combined retaining structure with different rock shapes. *Struct. Eng. Mech.* **2020**, *73*, 599–612.
4. Lin, Y.L.; Yang, X.; Yang, G.L.; Li, Y.; Zhao, L.H. A closed-form solution for seismic passive earth pressure behind a retaining wall supporting cohesive-frictional backfill. *Acta Geotech.* **2017**, *12*, 453–461. [\[CrossRef\]](#)
5. Rajaei, S.H.; Khodashenas, S.R.; Esmaili, K. Comparative evaluation of energy dissipation over short stepped gabion and rigid spillways. *J. Hydraul. Res.* **2020**, *58*, 262–273. [\[CrossRef\]](#)
6. Amato, G.; O'Brien, F.; Simms, C.K.; Ghosh, B. Multibody modelling of gabion beams for impact applications. *Int. J. Crash.* **2013**, *18*, 237–250. [\[CrossRef\]](#)
7. Smoltczyk, U.; Malcharek, K. Slope protection by membrane structures. *Geotext. Geomembr.* **1985**, *2*, 323–336. [\[CrossRef\]](#)
8. Bathurst, R.J.; Rajagopal, K. Large-scale triaxial compression testing of geocell reinforced granular soils. *Geotech. Test. J.* **1993**, *16*, 296–303.
9. Jayasree, P.K. Performance of Gabion Faced Reinforced Earth Retaining Walls. Ph.D. Thesis, Cochin University of Science and Technology, Kochi, India, 2008.
10. Muhunthan, B.; Shu, S.; Sasiharana, N.; Hattaleh, O.; Badger, T.C.; Lowell, S.M.; Duffy, J.D.; Center, W.S.T. *Analysis and Design of Wire Mesh/Cable Net Slope Protection*; California Department of Transportation: Sacramento, CA, USA, 2005.
11. Hsieh, C.W.; Chang, C.W.; Liu, I.W.; Liu, R.S. Structural Pattern Effects on Engineering Behavior of Hexagonal Wire Mesh Gabion Panels. *Transport. Res. Rec.* **2013**, *2349*, 3–8. [\[CrossRef\]](#)
12. Thoeni, K.; Lambert, C.; Giacomini, A.; Sloan, S.W. Discrete modelling of hexagonal wire meshes with a stochastically distorted contact model. *Comput. Geotech.* **2013**, *49*, 158–169. [\[CrossRef\]](#)
13. Bertrand, D.; Nicot, F.; Gotteland, P.; Lambert, S. Discrete element method (DEM) numerical modeling of double-twisted hexagonal mesh. *Can. Geotech. J.* **2008**, *45*, 1104–1117. [\[CrossRef\]](#)
14. Lambert, S.; Gotteland, P.; Nicot, F. Experimental study of the impact response of geocells as components of rockfall protection embankments. *Nat. Hazards Earth Syst. Sci.* **2009**, *9*, 459–467. [\[CrossRef\]](#)
15. Lin, Y.L.; Yang, G.L.; Li, Y.; Zhao, L.H. Engineering behaviors of reinforced gabion retaining wall based on laboratory test. *J. Cent. South Univ. Technol.* **2010**, *17*, 1351–1356. [\[CrossRef\]](#)
16. Bergado, D.T.; Youwai, S.; Teerawattanasuk, C.; Visudmedanukul, P. The interaction mechanism and behavior of hexagonal wire mesh reinforced embankment with silty sand backfill on soft clay. *Comput. Geotech.* **2003**, *30*, 517–534. [\[CrossRef\]](#)
17. Zhang, H.J.; Liu, G.N.; Liu, W.X.; Chen, Z.K.; Liu, Q.Y.; Xu, G.Y. Experimental study on failure mode and mechanical characteristics of gabion material. *Constr. Build. Mater.* **2022**, *344*, 128119. [\[CrossRef\]](#)
18. Atanasovska, I.; Momcilovic, D.; Gavrilovski, M. Development of the universal tool for testing of tensile properties of hexagonal steel wire mesh for Civil Engineering. *Metall. Mater. Eng.* **2018**, *24*, 113–122. [\[CrossRef\]](#)
19. Lin, Y.L.; Li, Y.X.; Zhao, L.H.; Yang, T.Y. Investigation on the seismic response of a three-stage soil slope supported by the anchor frame structure. *J. Cent. South Univ.* **2020**, *27*, 1290–1305. [\[CrossRef\]](#)
20. Lin, Y.L.; Lu, L.; Yang, G.L. Seismic behavior of a single-form lattice anchoring structure and a combined retaining structure supporting soil slope: A comparison. *Environ. Earth Sci.* **2020**, *79*, 78. [\[CrossRef\]](#)
21. Lin, Y.L.; Cheng, X.M.; Yang, G.L.; Li, Y. Seismic response of a sheet-pile wall with anchoring frame beam by numerical simulation and shaking table test. *Soil Dyn. Earthq. Eng.* **2018**, *115*, 352–364. [\[CrossRef\]](#)
22. Lin, Y.L.; Cheng, X.M.; Yang, G.L. Shaking table test and numerical simulation on a combined retaining structure response to earthquake loading. *Soil Dyn. Earthq. Eng.* **2018**, *108*, 29–45. [\[CrossRef\]](#)
23. Lin, Y.L.; Jin, J.; Jiang, Z.H.; Liu, W.; Liu, H.D.; Li, R.F.; Liu, X. Seismic response of combined retaining structure with inclined rock slope. *Struct. Eng. Mech.* **2022**, *84*, 591–604.
24. Lin, Y.L.; Li, Y.X.; Yang, G.L.; Li, Y. Experimental and numerical study on the seismic behavior of anchoring frame beam supporting soil slope on rock mass. *Soil Dyn. Earthq. Eng.* **2017**, *98*, 12–23. [\[CrossRef\]](#)
25. Ferro, R. Computer simulation of trawl gear shape and loading. In Proceedings of the Word Symposium on Fishing Gear and Fishing Vessel Design, St. John's, NL, Canada, 20–24 November 1988; pp. 259–262.
26. Gu, M.; Collin, J.G.; Han, J.; Zhang, Z.; Tanyu, B.F.; Leshchinsky, D.; Ling, H.I.; Rimoldi, P. Numerical analysis of instrumented mechanically stabilized gabion walls with large vertical reinforcement spacing. *Geotext. Geomembr.* **2017**, *45*, 294–306. [\[CrossRef\]](#)
27. Grodecki, M. Finite element modelling of the hexagonal wire mesh. *Arch. Civ. Eng.* **2020**, *66*, 705–720.
28. Cazzani, A.; Mongioli, L.; Frenez, T. Dynamic finite element analysis of interceptive devices for falling rocks. *Int. J. Rock Mech. Min. Sci.* **2002**, *39*, 303–321. [\[CrossRef\]](#)
29. Mummadisingh, J.V.; Sengupta, A. Study of the dynamic performance of a gabion wall. *Structures* **2023**, *50*, 576–589. [\[CrossRef\]](#)
30. Priour, D. Analysis of nets with hexagonal mesh using triangular elements. *Int. J. Numer. Meth. Eng.* **2003**, *56*, 1721–1733. [\[CrossRef\]](#)

31. Hussein, M.G.; Meguid, M.A. A three-dimensional finite element approach for modeling biaxial geogrid with application to geogrid-reinforced soils. *Geotext. Geomembr.* **2016**, *44*, 295–307. [[CrossRef](#)]
32. Chen, T.C.; Chen, R.H.; Lin, S.S. A nonlinear homogenized model applicable to reinforced soil analysis. *Geotext. Geomembr.* **2000**, *18*, 349–366. [[CrossRef](#)]
33. Bergado, D.T.; Voottipruex, P.; Srikongsri, A.; Teerawattanasuk, C. Analytical model of interaction between hexagonal wire mesh and silty sand backfill. *Can. Geotech. J.* **2001**, *38*, 782–795. [[CrossRef](#)]
34. Vangheluwe, L. Influence of strain rate and yarn number on tensile test results. *Text. Res. J.* **1992**, *62*, 586–589. [[CrossRef](#)]

Disclaimer/Publisher’s Note: The statements, opinions and data contained in all publications are solely those of the individual author(s) and contributor(s) and not of MDPI and/or the editor(s). MDPI and/or the editor(s) disclaim responsibility for any injury to people or property resulting from any ideas, methods, instructions or products referred to in the content.